

Soft X-ray spectroscopy of Compton-thick Seyfert 2 galaxies with BeppoSAX

M. Guainazzi¹, G. Matt², L.A. Antonelli³, L. Bassani⁴, A.C. Fabian⁵, R. Maiolino⁶,
A. Marconi⁶, F. Fiore^{3,7}, K. Iwasawa⁵, L. Piro⁸

¹*Astrophysics Division, Space Science Department of ESA, ESTEC, Postbus 299, NL-2200 AG Noordwijk, The Netherlands*

²*Dipartimento di Fisica “E. Amaldi”, Università degli Studi “Roma Tre”, Via della Vasca Navale 84, I-00146 Roma, Italy*

³*Osservatorio Astronomico di Roma, Via dell’Osservatorio, I-00144 Monteporzio Catone, Italy*

⁴*Istituto Tecnologie e Studio delle Radiazioni Extraterrestri, C.N.R., Via Gobetti 101, I-40129 Bologna, Italy*

⁵*Institute of Astronomy, University of Cambridge, Madingley Road, Cambridge CB3 0HA, United Kingdom*

⁶*Osservatorio Astrofisico di Arcetri, Largo E. Fermi 5, I-50125 Firenze, Italy*

⁷*BeppoSAX Science Data Center, Via Corcolle 19, I-00131 Roma, Italy*

⁸*Istituto di Astrofisica Spaziale, CNR, Via Fosso del Cavaliere, I-00133 Roma, Italy*

23 March 2022

ABSTRACT

We present a X-ray spectroscopic study of the bright Compton-thick Seyfert 2s NGC 1068 and Circinus Galaxy, performed with BeppoSAX. Matt et al. (1997 and 1998) interpreted the spectrum above 4 keV as the superposition of Compton reflection and warm plasma scattering of the nuclear radiation. When this continuum is extrapolated downwards to 0.1 keV, further components arise. The NGC 1068 spectrum is rich in emission lines, mainly due to K_α transitions of He-like elements from oxygen to iron, plus a K_α fluorescent line from neutral iron. If the ionized lines originate in the warm scatterer, its thermal and ionization structure must be complex. From the continuum and line properties, we estimate a column density, N_{warm} , of the warm scatterer less than a few $\times 10^{21} \text{ cm}^{-2}$. In Circinus Galaxy, the absence of highly ionized iron is consistent with a scattering medium with $U_X \lesssim 5$ and $N_{\text{warm}} \sim \text{a few} \times 10^{22} \text{ cm}^{-2}$. In both cases the neutral iron line is most naturally explained as fluorescence in the medium responsible for the Compton reflection continuum. In NGC 1068 an optically thin plasma emission with $kT \simeq 500 \text{ eV}$ and strongly sub-solar metallicity is required, while such a component is only marginal in Circinus Galaxy. We tentatively identify this component as emission of diffuse hot gas in the nuclear starbursts. Possible causes for the metal depletion are discussed.

Key words: Line: formation – galaxies: individual: NGC 1068, Circinus Galaxy – galaxies: active – X-rays: galaxies

1 INTRODUCTION

In the last fifteen years, a wide consensus has gathered around the idea that the nucleus and the Broad Line Region (BLR) in Seyfert 2s are hidden to us by intervening matter along the line of sight (see Antonucci 1993 for a review on unification models). While column densities $\approx 10^{22} - 10^{24} \text{ cm}^{-2}$ were measured by Ginga in most Seyfert 2s (Awaki et al. 1991; Smith & Done 1996), so confirming this hypothesis, no significant absorption in excess of the Galactic contribution was detected in some objects. A key to explain the nature of these apparently odd sources came from the evidence that they exhibit intense iron lines, strongly

suggesting that the observed X-ray emission is due to scattering of the nuclear radiation, which in turn is completely obscured. In fact, if the column density of the absorbing matter exceeds 10^{24} cm^{-2} , the nucleus is invisible up to at least 10 keV (and then no absorption would be directly observed). At least two possible candidates exist as reflectors: the inner side of the molecular torus (“cold reflector”) and the hot plasma responsible for the scattering of optical broad lines (“warm mirror” or “warm reflector”).

In the former case, the X-ray spectrum should be dominated by a “bare” Compton-reflection component (George & Fabian 1991; Ghisellini et al. 1994; Krolik et al. 1994) and an intense (equivalent width $EW \gtrsim 1 \text{ keV}$) K_α fluorescent

line from neutral or mildly ionized iron (Matt et al. 1999a, MBF96 hereinafter). This is indeed what has been observed in a handful of objects so far: NGC 1068 (the archetypical Seyfert 2 galaxy: Ueno et al. 1994; Iwasawa et al. 1997; Matt et al. 1997a, M97 hereinafter), NGC 6240 (Iwasawa & Comastri 1998); Circinus Galaxy (Matt et al. 1996b, Matt et al. 1999; M99 hereinafter); NGC 7674 (Malaguti et al. 1998); Mkn 3 (Turner et al. 1997a; Cappi et al. 1999). These objects constitute the set of so-called “Compton-thick” sources. Recent results from a BeppoSAX study of an optically-selected sample suggest that they are far more common than previously thought due to selection biases in the Seyfert 2 samples observed in X-rays before (Maiolino et al. 1998).

The X-ray continuum scattered by the warm material is instead a fainter replica of the nuclear non-thermal continuum (if self-absorption effects are not important), plus a set of emission lines from highly ionized heavy elements, which are produced by fluorescence/recombination and/or resonant scattering in the ionized matter (MBF96; Netzer 1996; Netzer et al. 1998, NTG98 hereinafter).

The X-ray observations, performed so far, suggest that both mechanisms are usually at work. Soft excesses above the extrapolation of the intermediate X-ray 2–10 keV power-laws have been revealed in 21 out of 25 Seyfert 2s observed by ASCA (Turner et al. 1997b), and in all “Compton-thick” sources (Turner et al. 1997b; Iwasawa & Comastri 1998; Matt et al. 1996b). Emission lines from He-, H-like iron and lighter elements have been detected in 4 out of 7 Compton-thick sources (Matt et al. 1996b; Turner et al. 1997b). Scattering models can generally account well for these soft excesses. However, a description of these features in terms of optically thin thermal emission often yields statistically comparable results. This is not surprising. Some studies indicate that the host galaxies of Seyfert 2s have high levels of star formation (Maiolino & Rieke 1995) and several examples of nuclear starbursts occurring in Seyfert 2s are known. The average contribution of starbursts to the 0.5–4.5 keV flux was estimated to be 60% in the sample of Seyfert 2s observed by ASCA (Turner et al. 1997b), although admittedly ASCA could not disentangle unambiguously the starburst from the scattered emission. In only one case a significant contribution from starburst could be ruled out (Mkn 3; Turner et al. 1997a).

High spatial resolution is required to separate the contribution of different spectral components and to perform spatially-resolved spectroscopy. Hopefully, this capability will be provided in the near future by the detectors on board *Chandra* and XMM. In the meantime, a wide enough spectral coverage can be exploited to separate the cold and warm reflection components above 3 keV and to quantify any contribution to the soft X-ray emission from a starburst component. The Italian-Dutch satellite BeppoSAX (Boella et al. 1997a), whose scientific payload covers the energy range between 0.1 and 200 keV, is the presently operating mission best suited for this purpose. For example it has allowed for the first time the measurement of the relative contributions of the cold and warm mirrors in NGC 1068, confirming the complex nature of the reflector, first suggested by ASCA spectroscopy of the iron line complex (Iwasawa et al. 1997). In this *paper* we will focus on the soft X-ray properties of NGC 1068 and Circinus Galaxy, which were observed by

BeppoSAX during a program of spectral survey of Compton-thick Seyfert 2s.

Both sources are very pertinent to the above discussion. In both of them, broad optical lines have been detected in polarized light (the degree of polarization being $\simeq 16\%$ in NGC 1068, Antonucci & Miller 1985; and $\simeq 2\%$ in Circinus Galaxy, Oliva et al. 1998). Both galaxies are site of strong starburst activity. In NGC 1068 the bulk of this activity is concentrated in a ring of approximately 1 kpc size [*i.e.*: 15–16” at the distance of 14.4 Mpc (Tully 1988)], which protrudes a bar towards the nucleus (Scoville 1988). The HRI image revealed that half of the X-ray emission at 0.8 keV comes from an extended region of $\simeq 13$ kpc scale (Wilson et al. 1992). It is worth remembering that NGC 1068 hosts a “water maser” source (Claussen et al. 1984), probably coincident with the inner region of a dusty, nearly edge-on torus at a distance of $\simeq 0.4$ pc from the nucleus (Greenhill et al. 1996).

Circinus Galaxy also exhibits a strong and variable H₂ maser emission (Greenhill et al. 1997), which instead may be produced in a $\lesssim 10$ AU Keplerian disk around the nucleus. Enhanced star formation activity in the shape of a ring is present on a $\simeq 200$ pc scale (corresponding to $\simeq 10''$ at the distance of 4 Mpc; Marconi et al. 1994). Although the total luminosity of the starburst within a few hundred pc is comparable to the intrinsic luminosity of the Seyfert nucleus, only 2% of it is radiated within the inner 12 pc (Maiolino et al. 1998a).

2 OBSERVATIONS, DATA REDUCTION AND PREPARATION

The Italian-Dutch satellite BeppoSAX (Boella et al. 1997a) carries four co-aligned Narrow Field Instruments. Two of them are gas scintillation proportional counters with imaging capabilities: the Low Energy Concentrator Spectrometer (LECS, 0.1–10 keV, Parmar et al. 1997) and the Medium Energy Concentrator Spectrometer (MECS, 1.8–10.5 keV, Boella et al. 1997b). They have an energy resolution of $\simeq 8\%$ at 6 keV (MECS) and of $\simeq 4\%$ at 1 keV (LECS). The other two instruments are collimated detectors, mounted on a rocking system to allow a continuous monitoring of the background: the High Pressure Gas Scintillator Proportional Counter (HPGSPC, 4–120 keV, Manzo et al. 1997) and the Phoswich Detector System (PDS, 13–200 keV). The HPGSPC is tuned for spectroscopy of bright sources with good energy resolution, while the PDS possesses an unprecedented sensitivity in its energy bandpass. Only LECS, MECS and PDS data will be considered in this *paper*, since the HPGSPC failed to detect both sources.

The NGC 1068 observation was interrupted after $\simeq 70\%$ of the scheduled exposure time and completed about one year later. The log of the observations is reported in Table 1. Data were reduced according to the same prescriptions as in M97. The only difference regards the PDS data, on which a crystal temperature dependent Rise Time threshold was applied during the screening procedure. By reducing the instrumental background by $\sim 50\%$, this method allowed an improvement in the S/N ratio from 4.5 to 8σ . We assume hereinafter that this also implies a decrease by a factor 0.92 of the effective area in comparison to the publicly available

Table 1. BeppoSAX observations log. T_{exp} and CR are the total effective exposure time and count rate in the 0.1–4 keV, 1.8–10.5 keV and 13–200 keV bands for the LECS, MECS and PDS, respectively.

Source	Start time (UTC)	End time (UTC)	$T_{\text{exp}}^{\text{LECS}}$ (s)	CR ^{LECS} (s ⁻¹)	$T_{\text{exp}}^{\text{MECS}}$ (s)	CR ^{MECS} (s ⁻¹)	$T_{\text{exp}}^{\text{PDS}}$ (s)	CR ^{PDS} (s ⁻¹)
NGC 1068 (1)	30/12/96 08:47:25	03/01/97 05:27:50	61497	0.1163 ± 0.0014	100150	0.0872 ± 0.0011	62493	0.18 ± 0.02
NGC 1068 (2)	11/01/98 09:52:36	12/01/98 08:07:50	15408	0.110 ± 0.03	37331	0.0664 ± 0.0015	17657	0.15 ± 0.06
CG	13/3/98 06:33:01	17/3/98 06:21:05	83853	0.0162 ± 0.0005	137700	0.0962 ± 0.0009	63200	2.01 ± 0.04

matrix (September 1997 release, Fiore et al. 1998), which were used throughout. Background spectra for the imaging instruments were extracted from blank field event files, using the same region in detector coordinates where the sources lie. PDS background subtracted spectra were obtained by plain subtraction of the “off-source” from the “on-source” ones. In all spectral fits, multiplicative factors were included to account for the absolute flux cross calibration misalignment between the BeppoSAX detectors (Grandi et al. 1997; Haardt et al. 1998). The LECS vs. MECS factor was left free to vary as a free parameter in the fits, and turned out to be $\simeq 0.9$. The PDS vs. MECS factor was fixed to 0.75. The results are not substantially affected by the residual $\lesssim 5\%$ uncertainty on the last parameter (Fiore et al. 1998).

In the following, errors are at the 90% confidence level for one interesting parameter (*i.e.*: $\Delta\chi^2 = 2.71$); energies are quoted in the source rest frame; $H_0 = 50 \text{ km s}^{-1} \text{ Mpc}^{-1}$, and cosmic abundance after Anders & Grevesse (1989) are assumed.

3 NGC 1068

Source spectra for NGC 1068 were extracted from circular regions of 8' and 6' radius for the LECS and MECS, respectively. The spectral analysis was performed in two steps. First, we re-analyzed the high-energy (*i.e.* above 4 keV) spectrum, to check the results of M97 after the improved PDS data screening algorithm and also to include the 1998 data set. Once the high-energy continuum shape was estimated, we tackled the task of describing the broadband spectrum. We have not found any difference in the spectral parameters larger than the statistical uncertainties between the 1996 and 1998 observations in any of the spectral model employed in this *paper*. The spectral analysis have therefore been performed on their union^{*} (“total” dataset hereinafter).

3.1 $E > 4 \text{ keV}$

In the analysis of the NGC 1068 spectra, we have followed the same approach as in M97. The MECS and PDS spectra above 4 keV have been fitted simultaneously with

^{*} The analysis of the total spectrum has been performed on the LECS and PDS summed spectra, while the MECS spectra of the two observations have been maintained separated and fitted simultaneously given the different number of operative MECS units (three versus two) between the two observations.

a model composed by a Compton reflection continuum (model **pexrav** in XSPEC, Magdziarz & Zdziarski 1995) and a power-law (describing the warm reflector component), both of them absorbed by the Galactic column density ($N_H = 3.1 \times 10^{20} \text{ cm}^{-2}$, Dickey & Lockman 1990). The photon index of the power-law and of the illuminating primary continuum, which gives rise to the Compton reflected component, were tied together. No cut-off has been assumed in the primary component. To describe the iron line complex we first tried a system of three narrow (*i.e.*: intrinsic width σ equal to 0) Gaussian lines; the centroid energy E of one of these components was held fixed to 6.4 keV (*i.e.*: fluorescence from neutral or mildly ionized iron) while the other two were left free to vary. The addition of a further narrow line yields a $\Delta\chi^2 = 8.3$ for two degrees of freedom, significant at more than 97.5% level of confidence, giving a line energy of $\simeq 8.1 \text{ keV}$. The quality of the fit is very good ($\chi^2 = 165.7/179 \text{ dof}$) and the photon spectral index ($\Gamma \simeq 2.0 \pm 0.2$) is consistent with that typically observed in Seyfert 1 galaxies (Nandra & Pounds 1994; Nandra et al. 1997). The best-fit solution requires the centroid energy of the K_α ionized iron lines to be $\simeq 6.56^{+0.12}_{-0.07} \text{ keV}$ (corresponding to $\text{FeXX}^{+\text{III}}_{-\text{II}}$) and $6.96^{+0.13}_{-0.08} \text{ keV}$ (Fe XXVI), with Equivalent Widths (EW) against the total continuum of 740 and 820 eV, respectively. The 8.1 keV line has a centroid energy consistent with the K_β transition from H-like iron ($E_c = 8.1 \pm 0.2 \text{ keV}$) and its ratio with the 6.96 keV line is 0.18 ± 0.12 . The MECS does not have enough energy resolution to allow a totally unambiguous deconvolution of the iron line complex in this source. Comparably good fits (albeit formally slightly worse) can be obtained also if one assumes a system of $\text{FeI}+6.61 \text{ keV}+6.86 \text{ keV}$ lines (as suggested by Iwasawa et al. 1997; $\chi^2 = 173.6/180 \text{ dof}$) or of $\text{FeI}+\text{FeXXV}+\text{FeXXVI}$ ($\chi^2 = 171.5/180 \text{ dof}$). The 8.1 keV line is required at comparable statistical significance in all the above deconvolutions. The relative weight of the K_α iron components varies significantly in the three models. In the following we will assume the last one as our baseline as it is the most physically reasonable. The properties of the lines in this scenario are reported in Table 3.

In Figure 1 the best-fit model and residuals photon spectrum is shown for the total dataset. It will be referred to as the “**double-reflector**” model hereinafter, whereas the **double-reflector continuum** will refer to the above model without the iron emission line complex.

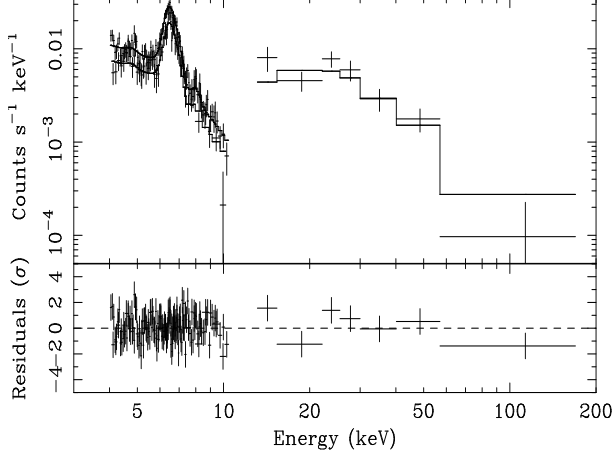


Figure 1. NGC 1068 spectra (*upper panel*) and residuals in units of standard deviations (*lower panel*) when the best-fit double-reflector model is applied to the MECS/PDS spectra above 4 keV

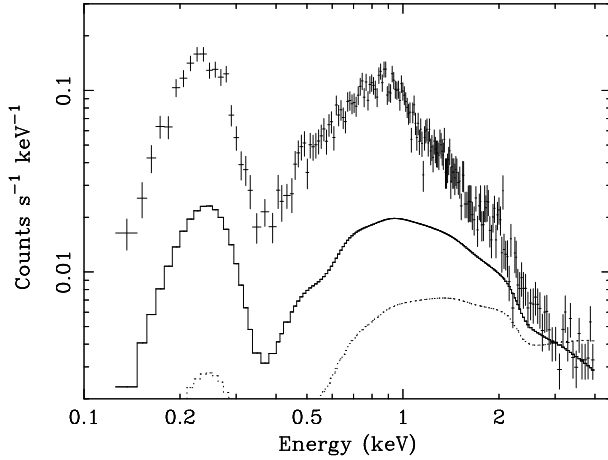


Figure 2. Extrapolation of the high-energy best-fit double-reflector model (*solid line*) in the LECS energy bandpass. Note the huge soft excess observed (*crosses*). The extrapolation of a power-law having the same flux at 4 keV but spectral index $\Gamma = 1.2$ (as observed by Ueno et al. (1994, *dotted line*)) is also shown for comparison

3.2 Broadband spectrum

In Figure 2, the extrapolation of the double-reflector model in the LECS band (below 4 keV) clearly shows the presence of a huge soft excess. Although this component has already been pointed out by several authors in the past (Marshall et al. 1993; Ueno et al. 1994), BeppoSAX unprecedented broadband coverage allows for the first time a self-consistent simultaneous study of *both* the hard emission and the soft excess properties. It is worth stressing that the soft excess is present despite the fact that the extrapolated spectrum is now much steeper than assumed so far. Previous studies have in fact calculated a mean intermediate X-ray spectrum and estimated the soft excess above it (cf. Figure 2). Now we can deconvolve the *observed* flat spectrum in two physical components.

We have modeled the soft excess by adding to the

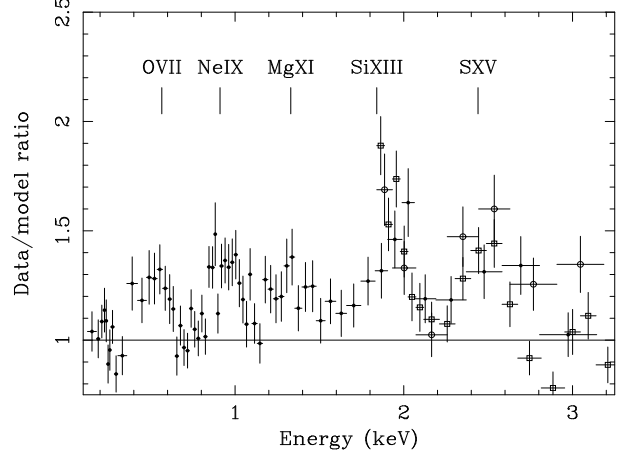


Figure 3. Data/model ratio when the double reflector model plus a thermal optically thin plasma is applied to the LECS (*filled circles*), MECS (*empty squares*, 1996 dataset; *empty circles*, 1998 dataset) and PDS spectra (not shown) simultaneously. The labels indicate the likely identification of the observed lines (marked at the expected energies after taking into account the redshift of the source). Each data point has a signal-to-noise ratio > 10

Table 2. Best-fit results obtained for NGC1068 when an extra component (indicated in the first row) is added to the double-reflector model in order to describe the observed soft excess. *po* = power-law; *br* = thermal bremsstrahlung; *mk* = optically thin plasma

Parameter	po	br	mk
N_H (10^{20} cm^{-2})	5.0 ± 0.4	3.1 ± 0.3	2.4 ± 0.4
Γ_{hard}	$2.30^{+0.11}_{-0.09}$	$2.12^{+0.17}_{-0.16}$	2.13 ± 0.17
Γ_{soft}	$3.21^{+0.13}_{-0.10}$		
$N_{\text{sc}}/N_{\text{pexrav}}$ (%)	< 1.2	7^{+3}_{-4}	7 ± 4
kT (eV)		410^{+40}_{-30}	440 ± 50
A_Z (%)			2.8 ± 1.6
χ^2/dof	513.0/442	453.7/440	451.3/441

double-reflector model a thermal plasma emission (model **mekal** in XSPEC), or a bremsstrahlung or a power-law. Although the quality of the fit improves dramatically in each case, local wiggles can still be seen both in the LECS and in the MECS spectrum (see Figure 3), suggesting that localized emission features are required by the data as well. We have therefore followed the approach of adding narrow Gaussian lines, until statistically required by the fit at the 99% significance level. This yields a system of five soft X-ray lines in the range 0.5–2.5 keV. The best-fit continuum and line parameters are shown in Table 2 and 3, respectively.

When the soft excess is modeled with an optically thin plasma, the χ^2 is rather good ($\chi^2_\nu = 1.02$). The addition of a further thermal component with a different temperature is not statistically required by the data ($\Delta\chi^2 < 0.1$). Note that the nuclear power-law index remains consistent with that typically observed in Seyfert 1 galaxies, although formally slightly steeper than the value obtained when the high-energy spectrum alone is analyzed. The thermal com-

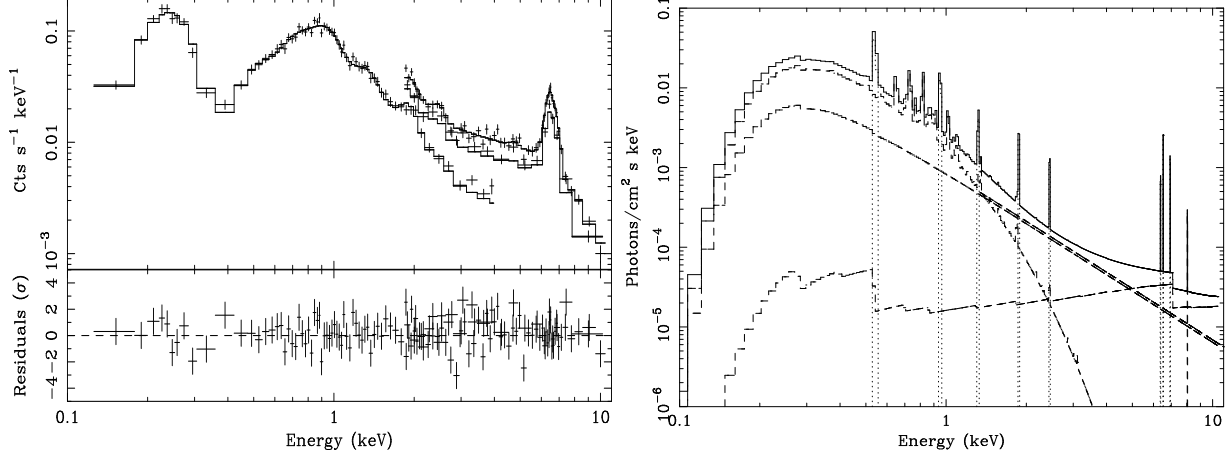


Figure 4. *Left panel:* Spectra and residuals in units of standard deviations when the best-fit model (double reflector model plus optically thin plasma) is applied to the broadband NGC 1068 spectrum (only LECS and MECS data are shown for clarity). Each data point has a signal-to-noise ratio > 10 . *Right panel:* inferred best fit model. The *Solid line* represents the total spectrum, the *dashed lines* the continuum spectral components and the *dotted lines* the emission lines

ponent best-fit abundance is strongly sub-solar ($\simeq 3\%$), the temperature is $\simeq 440$ eV and the unabsorbed total luminosity is $\sim 9.3 \times 10^{41}$ erg s $^{-1}$ (0.1–10 keV). The best-fit line centroid energies are 0.54, 0.95, 1.32, 1.88, 2.45 keV, and are consistent (within the statistical uncertainties) with K_{α} fluorescence of He-like oxygen, neon, magnesium, silicon and sulphur (*i.e.*: OVII, NeIX, MgXI, SiXII, SXV) (see Table 3). The best-fit results and model are shown in Figure 4. The thermal component contributes substantially only to the iron-L complex. The soft X-ray lines EW against the *total* continuum are in the range 70–180 eV, while against the *scattered* continuum are in the range 130–340 eV.

The total observed fluxes in the 0.1–2 and 2–10 keV bands are 1.11 and 0.52×10^{-11} erg cm $^{-2}$ s $^{-1}$ in the 0.1–2 and 2–10 keV bands, respectively. They correspond to unabsorbed rest frame luminosities of 1.31 and 0.38×10^{42} erg s $^{-1}$. The relative fluxes (2–10 keV band) of the Compton reflection and scattering components are 1.9 and 2.2×10^{-12} erg s $^{-1}$ cm $^{-2}$, corresponding to unabsorbed luminosities of 1.34 and 1.55×10^{41} erg s $^{-1}$, respectively.

The abundance of the best-fit *mekal* model in the above scenario is very low and the contribution to the observed soft X-ray emission lines is therefore in most cases negligible. We, therefore, repeated the fit, assuming this time that the soft excess is simply due to a featureless continuum component, either a thermal bremsstrahlung or a power law (even though these models could not be physically plausible). The best-fit results and parameters are shown again in Tables 2 and 3. In the thermal bremsstrahlung case, the main difference is that a line at $E \simeq 0.78$ keV is significantly required, to account for the missing *mekal* contribution to the iron-L complex (see Figure 4). This new line has an EW of $\simeq 100$ eV (380 eV) against the total (scattered) continuum. Not surprisingly, the other best fit parameters are very close to those obtained in the optically thin plasma scenario. By contrast, a much worse fit is obtained if instead a power-law is used to model the soft excess (only an upper limit on the scattering fraction can be set in this case). The fit is unacceptable at $\gtrsim 98\%$ level of confidence ($\chi^2_{\nu} = 1.16$ for 442 dof) and

the steeper index obtained for the intrinsic nuclear emission ($\Gamma \simeq 2.3$) produces a systematic underestimate of the PDS counts.

It is worth noticing that an unacceptable fit is obtained ($\chi^2 = 900.1/448$ dof) if we abandon the double-reflector scenario and assume that the soft excess (above a bare Compton reflection) *and* the lines from ionized species are accounted for by several single-temperatures optically thin regions. Similar results are obtained if one adopts a single multi-temperature emission plasma. This provides a further indirect confirmation of the validity of the high-energy spectral deconvolution.

4 CIRCINUS GALAXY

4.1 BeppoSAX data

The ASCA 0.5–10 keV spectrum of the Circinus Galaxy is well fitted by a bare Compton-reflection component, a soft excess and a system of emission lines (Matt et al. 1996b). The BeppoSAX observation has permitted to discover that at energies above ~ 10 keV the primary continuum emerges, suggesting that the nuclear region is seen through a screen of absorbing matter with $N_H \sim 4 \times 10^{24}$ cm $^{-2}$. The reader is referred to M99 for a detailed study of the high-energy spectrum. In the following we will focus on the soft excess and emission line system. Only LECS and MECS data will be considered in the following, since PDS data are largely affected by the transmitted component, whose contribution is instead negligible in the 0.1–10 keV band. For the data reduction see M99. Source spectra have been extracted from circular regions of $2'$ radius around the source image centroid, to avoid contamination from a serendipitous source in the field of view (M99).

The available statistics below 2 keV is limited by the relatively large Galactic absorption ($N_{H,Gal} \sim 3 \times 10^{21}$ cm $^{-2}$, Dickey & Lockman 1990). There is therefore less room than in NGC 1068 for deconvolving the soft X-ray spectral complexity and/or to perform a detailed line spectroscopy

Table 3. X-ray lines detected in NGC 1068. Centroid energies are in keV, EW in eV. $EW_{\text{tot}}^{(i)}$ is the equivalent width against the total continuum, $EW_{\text{sc}}^{(i)}$ against the warm scattered continuum only, $EW_{\text{cr}}^{(i)}$ against the Compton-reflection continuum only. The third column indicates the most likely identification. In brackets the line fluxes are quoted in units of photons $\text{cm}^{-2} \text{s}^{-1}$. The properties of the iron line complex are here given for the FeI+FeXXV+FeXXVI plus the $\simeq 8.1$ keV line deconvolution. All lines refer to K_{α} transitions, unless otherwise specified.

Parameter	br	mk	Identification
$E^{(1)}$	0.59 ± 0.04	0.54 ± 0.04	O VII
$EW_{\text{tot}}^{(1)}$	$80 \pm_{40}^{90}$	70 ± 30	(1.0×10^{-3})
$EW_{\text{sc}}^{(1)}$	$340 \pm_{150}^{380}$	310 ± 140	
$E^{(2)}$	$0.78 \pm_{0.04}^{0.06}$	0.78^{\dagger}	Fe-L
$EW_{\text{tot}}^{(2)}$	100 ± 30	< 50	
$EW_{\text{sc}}^{(2)}$	380 ± 110	< 180	
$E^{(3)}$	$0.95 \pm_{0.02}^{0.04}$	0.95 ± 0.03	Ne IX
$EW_{\text{tot}}^{(3)}$	$150 \pm_{40}^{50}$	90 ± 30	(3.3×10^{-4})
$EW_{\text{sc}}^{(3)}$	$480 \pm_{140}^{170}$	320 ± 100	
$E^{(4)}$	$1.32 \pm_{0.05}^{0.06}$	1.32 ± 0.05	Mg XI
$EW_{\text{tot}}^{(4)}$	80 ± 30	70 ± 30	(8.7×10^{-5})
$EW_{\text{sc}}^{(4)}$	180 ± 70	170 ± 70	
$E^{(5)}$	$1.88 \pm_{0.02}^{0.03}$	1.88 ± 0.03	Si XIII
$EW_{\text{tot}}^{(5)}$	$180 \pm_{30}^{40}$	170 ± 40	(6.9×10^{-5})
$EW_{\text{sc}}^{(5)}$	$280 \pm_{40}^{70}$	280 ± 60	
$E^{(6)}$	$2.46 \pm_{0.04}^{0.03}$	2.45 ± 0.04	S XV
$EW_{\text{tot}}^{(6)}$	160 ± 40	160 ± 40	(3.1×10^{-5})
$EW_{\text{sc}}^{(6)}$	220 ± 50	210 ± 50	
$E^{(7)}$	6.7^{\dagger}		Fe XXV
$EW_{\text{tot}}^{(7)}$	1000 ± 200		(5.4×10^{-5})
$EW_{\text{sc}}^{(7)}$	3000 ± 600		
$E^{(8)}$	6.96^{\dagger}		Fe XXVI
$EW_{\text{tot}}^{(8)}$	$530 \pm_{170}^{140}$		(2.5×10^{-5})
$EW_{\text{sc}}^{(8)}$	$1500 \pm_{500}^{400}$		
$E^{(9)}$	8.1 ± 0.2		Fe XXVI (K_{β})
$EW_{\text{tot}}^{(9)}$	230 ± 130		(7.0×10^{-6})
$EW_{\text{sc}}^{(9)}$	600 ± 300		
$E^{(10)}$	6.4^{\dagger}		Fe I–XVI
$EW_{\text{tot}}^{(10)}$	1000 ± 140		(5.5×10^{-5})
$EW_{\text{cr}}^{(10)}$	1600 ± 200		

† fixed

A rather bad fit is obtained if a double-reflector continuum plus an iron K_{α} fluorescent line is used ($\chi^2 = 594.2/78$ dof, see Figure 5). Most of the residuals are due to several unaccounted emission lines. We then added narrow lines one-by-one, until required in terms of F-test statistics at 99% confidence level. Eventually, six lines were needed, with best-fit centroid energies of 1.87, 2.44, 3.14, 6.45, 7.09, and 7.9 keV (see Table 4). The most likely identifications for the first five lines are K_{α} fluorescence of Si XIII, S XV, Ar XVII, Fe XVII–XIX, and Fe XXV (or Ni K_{α}), respectively. Most of them had already been measured in the ASCA ob-

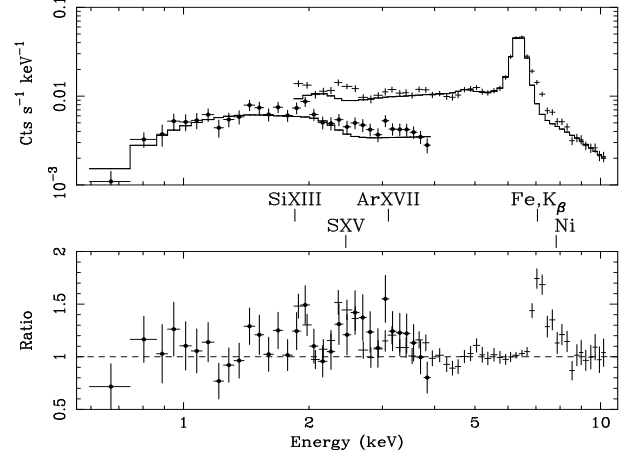


Figure 5. Spectra (*upper panel*) and residuals in units of standard deviations (*lower panel*), if the double-reflector continuum + one Gaussian iron fluorescent K_{α} line model is applied to the LECS (*filled circles*) and MECS (*crosses*) spectra of Circinus Galaxy. Most likely identification of the residual line features are labeled. All lines refers to K_{α} transitions if not otherwise stated

Table 4. Same as Table 3 for Circinus Galaxy.

$E^{(1)}$	$1.87 \pm_{0.05}^{0.04}$	Si XIII
$EW_{\text{tot}}^{(1)}$	$120 \pm_{50}^{60}$	(3.4×10^{-5})
$EW_{\text{sc}}^{(1)}$	$160 \pm_{60}^{80}$	
$E^{(2)}$	$2.43 \pm_{0.04}^{0.05}$	S XV
$EW_{\text{tot}}^{(2)}$	190 ± 50	(4.0×10^{-5})
$EW_{\text{sc}}^{(2)}$	260 ± 70	
$E^{(3)}$	$3.14 \pm_{0.09}^{0.11}$	Ar XVII
$EW_{\text{tot}}^{(3)}$	$90 \pm_{50}^{40}$	(1.5×10^{-5})
$EW_{\text{sc}}^{(3)}$	$140 \pm_{80}^{60}$	
$E^{(4)}$	$6.446 \pm_{0.013}^{0.012}$	Fe XVII–XIX
$EW_{\text{tot}}^{(4)}$	2250 ± 100	(3.19×10^{-4})
$EW_{\text{cr}}^{(4)}$	2850 ± 130	
$E^{(5)}$	7.08 ± 0.06	“Neutral” iron (K_{β})
$EW_{\text{tot}}^{(5)}$	$500 \pm_{90}^{80}$	(6.1×10^{-5})
$EW_{\text{cr}}^{(5)}$	$640 \pm_{110}^{100}$	
$E^{(6)}$	$7.9 \pm_{0.3}^{0.2}$	Fe XXV (or Ni K_{α})
$EW_{\text{tot}}^{(6)}$	180 ± 90	(1.6×10^{-5})
$EW_{\text{sc}}^{(6)}$	700 ± 300	
$EW_{\text{cr}}^{(6)}$	240 ± 120	

servation of Circinus Galaxy, with comparable EW (Matt et al. 1996b). It is worth noticing that the $\simeq 7.09$ keV line is inconsistent, given the uncertainties, with being produced by fluorescence of Fe XXVI, resolving an ambiguity that was still present in the ASCA data. The huge ($EW \simeq 2.3$ keV) line from neutral or mildly ionized iron is well consistent with being produced in the same cold reflector, whose emission dominates the 2–10 keV spectrum (Matt et al. 1996b).

The identification of the $\simeq 7.9$ keV line is not straightforward. In principle, it could be associated with K_{β} fluo-

rescence from He-like iron. If this is the case, one should expect a substantial contribution from the K_α line of this ion as well. Only a 90% upper limit of 52 eV can be set on the EW of a 6.7 keV line (against the total continuum), implying a K_β/K_α intensity ratio >0.22 . Alternatively, the line can be due to K_α fluorescence of nickel. The implied ionization state is still rather high ($>\text{NiXX}$). Again, one should expect for consistency a significant line contribution from K_α fluorescence of H-like iron at 6.96 keV. The 6.45 keV K_α line profile is narrow, the 90% upper limit on its intrinsic width being only 60 eV. This excludes in principle any significant blending with lines produced by ions more ionized than FeXX. The 90% upper limit on the EW (against the scattering continuum only) of a 6.96 keV narrow line is 530 eV, implying an implausible value of the ionized nickel versus ionized iron line ratio $\gtrsim 0.65$. The accuracy in the MECS instrumental gain reconstruction is $\lesssim 0.3\%$, and therefore comparable with or even slightly worse than the statistical uncertainties, but not enough to confuse the observed K_α iron line with that expected from an H-like stage. Future high resolution, large sensitivity observations are needed to allow a more definite conclusion on the identification of such a feature.

The ratio between the neutral/mildly ionized iron K_β and K_α intensities is 0.19 ± 0.04 , therefore slightly higher than expected from neutral matter (0.11, Kikoin 1976). The K_β line energy overlaps with the strong absorption edge associated with the Compton reflection component. Any small change in the detailed shape of the edge (due, for example, to a low degree of ionization of the reflector that might smear the edge shape) could have a significant effect on the K_β line intensity. We have tested this possibility using the model **pexriv** in XSPEC (Magdziarz & Zdziarski 1995), which takes self-consistently into account the ionization structure of the reflector. We have fixed the temperature to the value 10^5 K to avoid over-fitting the data, thus leaving only the ionization parameter (ξ) free. The improvement in the quality of the fit is very low ($\Delta\chi^2 = 0.8$) and the ionization parameter is very loosely constrained [$\log(\xi) = 0.0 \pm_{-1.4}^{+1.8}$]. Nonetheless, the K_β/K_α intensity ratio becomes $0.15 \pm_{0.05}^{+0.08}$, consistent with the expectations. This may be a further piece of evidence in favor of the idea that the cold reflector in Circinus Galaxy is actually mildly ionized. Alternatively, if the iron abundance is larger than solar, the intensity of the 7.09 keV line could be overestimated to compensate for the missing continuum photons above the photoelectric edge of neutral iron. Interestingly enough, an iron overabundance by a factor of about three is independently suggested by the EW of the K_α line (see Sect. 5.1). However, if we leave the iron abundance free to vary in the fit, no improvement is obtained, the K_β versus K_α intensity ratio remaining basically unchanged, and $Z_{\text{Fe}} = 0.9 \pm_{0.3}^{+1.4}$.

The $\simeq 3.14$ keV ArXVII line observed by BeppoSAX escaped detection in the ASCA data. We stress here that the exposure time of the BeppoSAX observation is about four times higher than the ASCA one. On the other hand, two lines seen by ASCA have not been detected by the LECS (at $\simeq 0.8$ keV and at $\simeq 1.33$ keV (Mgx-XI)), not surprisingly, given the larger ASCA sensitivity at these energies. The corresponding BeppoSAX 90% upper limits on the equivalent widths (121 and 53 eV, respectively) are, however, consistent with the ASCA values (Matt et al. 1996b).

Table 6. Serendipitous sources detected in the ROSAT/HRI observation of the sky region containing the Circinus Galaxy

Source #	R.A.(J2000)	Dec.(J2000)	Count Rate (s ⁻¹)
1	14 13 09.5	-65 20 14.8	0.0128 ± 0.0019
2	14 13 07.5	-65 20 06.4	0.0030 ± 0.0010
3	14 13 12.0	-65 20 07.5	0.0039 ± 0.0011
4	14 12 38.8	-65 23 30.7	0.0167 ± 0.0022

In Figure 6 the spectra, best-fit model (double reflector continuum plus emission lines) and residuals are shown in Figure 6. As already observed by M99 the best-fit photon index of the primary continuum ($\simeq 1.6$; see Table 5), is slightly flatter than that typically observed in Seyfert 1 galaxies, albeit not inconsistent given the relatively large uncertainties. The total observed fluxes in the 0.1–2 and 2–10 keV energy bands are 8.7×10^{-13} and 1.37×10^{-11} erg cm⁻² s⁻¹, corresponding to unabsorbed luminosities of 2.9×10^{40} and 1.34×10^{41} erg s⁻¹, respectively. The 2–10 keV band fluxes of the Compton reflection and scattering components are 6.3 and 3.0×10^{-12} erg s⁻¹ cm⁻², corresponding to unabsorbed luminosities of 6.0 and 2.9×10^{40} erg s⁻¹.

If a single temperature **mekal** model is added to the best-fit double reflector continuum plus lines model, a marginal improvement in the quality of the fit is obtained ($\Delta\chi^2 = 3.8$ for two more free parameters). The Compton-reflection, scattering and line properties are not substantially affected by the inclusion of this further component. The unabsorbed 0.1–10 keV luminosity corresponding to the best-fit nominal temperature ($\simeq 500$ eV) is 1.4×10^{40} erg s⁻¹, while the abundance is basically unconstrained.

No significant improvement in the quality of the fit is obtained if the optically thin plasma is substituted by a bremsstrahlung or if the soft X-ray power-law spectral index is left free to vary. Again, neglecting the double-reflector scenario and assuming that the whole soft excess and the ionized lines are due to a single or multi-temperature optically thin plasma yields an unacceptable χ^2 (98.0/69 dof).

4.2 HRI data

Contrary to NGC 1068, little can be found in the literature about the X-ray imaging of the Circinus Galaxy. For this reason, we present here the results of the only ROSAT/HRI observation (spatial resolution $\simeq 10''$ Full Width Half Maximum and 2-band spectral resolution in the nominal 0.1–2.4 keV energy bandpass), whose data are publicly available. The observation was performed from September 14 to 15, 1995 for a total exposure time of about 4200 seconds. Data were retrieved as event list from the HEASARC public archive, images were extracted with XSELECT and analyzed using the XIMAGE package (Giommi et al. 1991). PHA channels between 2 and 12 (approximately 0.1 and 2 keV) were used to optimize the signal to noise ratio; only data with a good attitude reconstruction were used.

Four X-ray sources are detected at more than 3σ level in the HRI field of view (see Table 6 and also Figure 7). Source #1 is very close to the optical position of Circinus galaxy

Table 5. Best-fit results of the Circinus galaxy 0.1–10 keV fits to continuum parameters in: (first row) the double reflector continuum plus emission lines model and (second row) the same model plus a thermal plasma.

Model	N_H 10^{20} cm^{-2}	Γ	N_{sc}/N_{pexrav} (%)	kT (keV)	Z (%)	χ^2/dof
po	25 ± 7	1.6 ± 0.2	$3.1^{+2.1}_{-1.1}$			58.7/67
po+mekal	80^{+60}_{-50}	$1.6^{+0.2}_{-0.3}$	$3.8^{+4.7}_{-1.6}$	$0.5^{+0.7}_{-0.3}$	100 [†]	54.9/65

[†] fixed

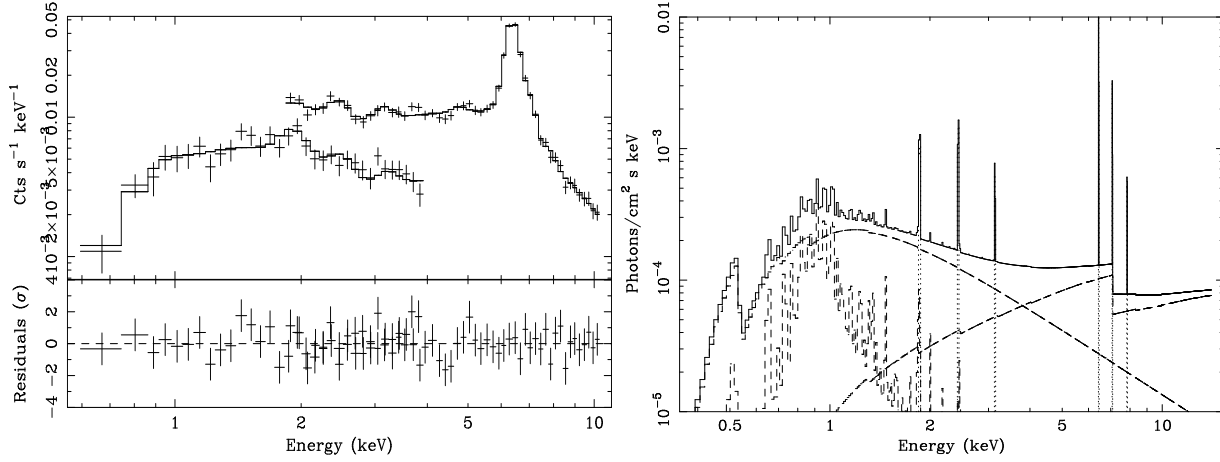


Figure 6. *Left panel:* Spectra and residuals in units of standard deviations when the best-fit model (double reflector continuum plus emission lines) is applied to the broadband Circinus Galaxy spectrum. Each data point has a signal-to-noise ratio > 10 . *Right panel:* inferred best fit model. The *Solid line* represents the total spectrum, the *dashed lines* the continuum spectral components and the *dotted lines* the emission lines.

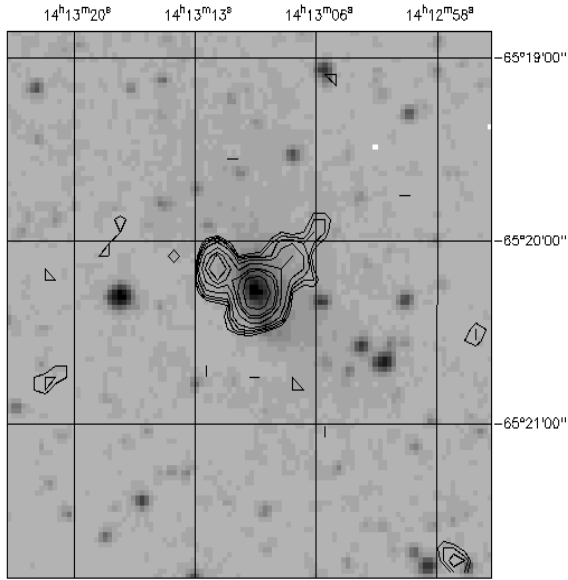


Figure 7. Zoom of the central 10 arcmin region of ROSAT/HRI field of view containing the Circinus Galaxy field (*contours*), superimposed to an optical plate

nucleus, allowing the identification of this X-ray source with the AGN. Sources #2 and #3 are 30–40 arcsec away from the nuclear region, while source #4 is located about 5 arcmin from the galaxy in the S-W direction. This last source was also detected by ASCA (Matt et al. 1996b) and BeppoSAX (M99).

No extended emission is detected around the nucleus. If we subtract the two sources closer to the nucleus, the residual nuclear emission is consistent with the PSF of the instrument (Davis et al. 1996). We stress, however, that the available exposure time is rather low and more statistics is needed before reaching a firm conclusion on this point. The flux of source #1 is $\simeq 4.2 \times 10^{-13} \text{ erg cm}^{-2} \text{ s}^{-2}$, which is about half of that observed by BeppoSAX. Sources #2 and #3 lie well within the extraction radius used for the BeppoSAX observation and could in principle contaminate the soft X-ray flux. If they are not variable, such a contamination could be as high as 25%, and therefore account for a substantial fraction of the galaxy soft excess. Although the possibility that the soft X-ray flux in the BeppoSAX data is entirely to one of these serendipitous sources cannot be ruled out *a priori*, it would however require that at least one of these sources varies by almost an order of magnitude up to a luminosity level $\gtrsim 10^{40} \text{ erg s}^{-1}$, while keeping coincidentally a $\Gamma \simeq 1.5$. Although we cannot reject this hypothesis on the basis of BeppoSAX (or ASCA) data alone,

we consider it almost unlikely and do not discuss it in the following.

5 DISCUSSION

5.1 X-ray lines

The BeppoSAX observations of NGC 1068 and Circinus galaxy have shown line-rich X-ray spectra. The lines are generally associated with He- or H-like ions of elements heavier than oxygen, the iron-L complex, and K_α (and, possibly K_β) fluorescent lines from neutral or mildly ionized iron. Similar lines had already been observed by BBXRT and ASCA, and most often associated with reprocessing of the primary radiation in the nuclear environment (Marshall et al. 1993; Turner et al. 1996b; Netzer & Turner 1997, M97). The energy resolution of the imaging instruments on-board BeppoSAX is not as good as that of the CCD on board ASCA and this limits its capability of deconvolving the K-shell iron line complex. However, at least two new results emerge from the BeppoSAX spectroscopy: i) the detection of emission lines around 8 keV, where BeppoSAX instruments can take advantage of a better effective area and comparable or lower background than the ASCA SIS; ii) the detection of a $\simeq 0.57$ keV line in NGC 1068, which is most likely due to the K_α fluorescence from He-like oxygen. The lack of the latter feature in previous spectra had forced to assume *ad hoc* oxygen-poor plasma (Marshall et al. 1993; Netzer & Turner 1997) in modeling the NGC 1068 warm mirror. This problem has now been overcome, given the accurate calibration of the LECS instrument on-board BeppoSAX around 0.5 keV (cf. Haardt et al. 1998; Orr et al. 1998).

A common feature of the spectra presented here is that the line contribution from any thermal plasma is negligible, with the possible exception of the iron-L complex (cf. Figure 4 and 6). This has implications on the nature of this spectral component which we tentatively associate with the nuclear starburst and discuss in the next section. In this section, instead, we will focus on the properties of all the other lines, which we assume to originate as fluorescence/recombination or resonant scattering from the cold and warm reflectors.

K_α (and K_β) fluorescent lines from neutral or mildly ionized iron are likely to originate in the cold reflector. In Circinus Galaxy, the lack of ionized iron lines allows a relatively unambiguous identification and deconvolution of the iron emission line complex. The observed K_α EW of $\simeq 2.3$ keV is in good agreement with the one measured by ASCA (M97) and corresponds to a value of $\simeq 2.8$ keV if measured against the Compton-reflection continuum alone. This value, coupled with the relatively low inclination angle ($i \lesssim 40^\circ$) derived from the hard X-ray analysis (M99), implies an iron overabundance by at least a factor of 3 (MBF96, Matt et al. 1997b). A K_β line is detected as well, with a ratio to the K_α line consistent with that expected on theoretical grounds, especially when a possible mild ionization of the reflecting medium is taken into account. The situation of NGC 1068 is far more complex. The limited MECS energy resolution does not allow to unambiguously deconvolve the line complex. We have assumed in the above analysis the reasonable hypothesis that the line is given by the superposition of a “neutral”, a He-like and a H-like component. In this

hypothesis, the EW of the neutral line against the Compton-reflection continuum is $\simeq 1.6$ keV. Following MBF96, this would suggest a high inclination (in agreement with the idea that the line comes from the same region as the water maser at $i \gtrsim 82^\circ$), but the large uncertainties on this value prevent any conclusion on this point.

The other lines observed correspond to He-like K_α transitions from O, Ne, Mg, Si, S, Fe and H-like Fe. Recent works have focused on producing self-consistent models for the lines expected from a plasma, photoionized by a strongly absorbed Seyfert-like continuum. In the following we will mainly refer to the works by Netzer & Turner (1997) and NTG98 and define the ionization parameter U_X as the dimensionless ratio between the ionizing photon flux (integrated in the 0.1–10 keV energy band) and the electron density (George et al. 1998). The calculations used in these papers take into account both the fluorescence/recombination and the resonance scattering lines, the latter process being dominant at densities $\lesssim 10^{22} \text{ cm}^{-2}$. We first consider the more complex case of NGC 1068. The wide range of ionized species observed can be hardly reconciled with a single-zone, homogeneous plasma. Assuming a density $N_{H,\text{warm}} = 2.5 \times 10^{22} \text{ cm}^{-2}$, all the lines from intermediate elements require $0.5 \leq U_X \leq 5$, except for the oxygen one (cf. Fig. 2 of NTG98). On the other hand, the highly ionized iron lines require $U_X \geq 5$. At this high level of ionization, oxygen is likely to be at least in H-like state, if not fully stripped. An intense OVII line is instead still consistent with neutral iron, requiring $U_X \leq 0.5$. We therefore conclude that the warm mirror must be complex and structured. At least three components are needed in NGC 1068, unless the oxygen line originates in the same cold reflector as the neutral iron lines. In Circinus Galaxy, the lack of detection of oxygen and highly ionized iron lines overcomes these difficulties, and the observed set of ionized lines can be easily explained with a single-zone scatterer with intermediate ionization parameter. However, while any contribution from a strongly ionized scatterer is ruled out, oxygen (and magnesium) lines are likely to have missed detection due to the higher Galactic neutral absorption along the line of sight. Actually, ASCA revealed a MgIX line, with an EW of about 90 eV (Matt et al. 1996b), which is consistent with the upper limit derived from the BeppoSAX data.

5.2 Some numbers on the reflectors

For a geometry such as that adopted by Ghisellini et al. (1994), the amount of cold reflection depends mainly on the inclination angle, while that of the ionized scattering depends almost entirely on the optical depth (or column density) of the scattering material (MBF96). From the 2–10 keV flux ratio of the warm vs cold reflection, we may therefore derive a relation between i and $N_{H,\text{warm}}$, which is shown in Fig. 8.

In the NGC 1068 case, the source is likely to be observed at very high inclination angles, as also implied by water maser measurements (Greenhill et al. 1996) and by the amount of cold reflection continuum measured (M97). Then $N_{H,\text{warm}}$ is constrained to be lower than, say, a few $\times 10^{21} \text{ cm}^{-2}$. An independent estimate of $N_{H,\text{warm}}$ can be derived from the equivalent widths of the ionized lines (with respect to the warm scattering continuum). These values (~ 3 keV

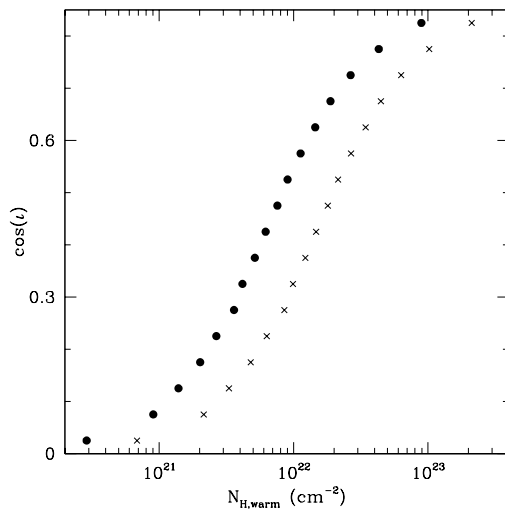


Figure 8. $\cos i$ vs. $N_{\text{H,warm}}$ relation in NGC 1068 (crosses) and Circinus Galaxy (filled circles)

and ~ 1.5 keV for the He- and H-like ions, respectively) may be compared with Figs. 4, 5 and 6 of MBF96, where the EW of these two ions are shown as a function of $N_{\text{H,warm}}$ (the total line EW decreases with $N_{\text{H,warm}}$ because the resonant scattering line becomes more and more optically thick). The values in those figures are for solar abundances and fraction of ions equal to 1. The value of the EW of the cold iron line (with respect to the Compton reflection) implies that the iron abundance is roughly solar (MBF96). Assuming typical ion fractions of $\lesssim 0.5$, the comparison of observed and expected EW yields $N_{\text{H,warm}}$ values lower than 10^{21} cm^{-2} , even allowing for turbulent motions in the matter (which reduce the line opacity). The EW of the other ionized lines are much lower than that of iron, but they are probably calculated against the *wrong* continuum and so not much information can be gathered from them. In any case, it must be stressed that the above calculation is not self consistent due to the presence of mildly ionized material responsible for the intermediate Z lines; instruments with much larger sensitivity and far better energy resolution are necessary to make any further progress in understanding the geometry and physics of the nuclear environment of NGC 1068.

The same calculation can be applied to Circinus Galaxy. If we assume that the inclination angle is $\lesssim 40^\circ$ (M99), the density of the warm scatterer has to be higher than a few 10^{22} cm^{-2} . This is in good agreement both with the value derived from the Sxv line EW (NTG98) and with the lack of detection of highly ionized iron lines (but the 90% upper limits on the EW of the He- or H-like iron lines are ~ 1.5 keV, i.e. consistent with practically any column density). The intrinsic luminosity is given by $L_X(2-10\text{keV}) \sim \frac{L_{\text{sc}}}{\tau \Delta\Omega/4\pi}$, where $\Delta\Omega$ is the solid angle subtended by the visible part of the illuminated ionized matter. From the hard X-ray spectrum, M99 derives $L_X(2-10\text{keV}) \sim 10^{42} \text{ erg s}^{-1}$, which implies $\tau \Delta\Omega/4\pi \sim 0.008$. In order to have, say, $N_{\text{H,warm}} = 3 \times 10^{22} \text{ cm}^{-2}$, $\Delta\Omega/4\pi$ should be ~ 0.3 , corresponding to an half-opening angle of the torus of $\simeq 65^\circ$.

A $N_{\text{H,warm}} \sim 10^{22} \text{ cm}^{-2}$ scatterer should also imprint

absorption features in the soft X-ray spectrum. The addition of photoionization absorption edges does not improve the quality of the fit in either NGC 1068 or Circinus Galaxy. The upper limits on the optical depths of OVII and OVIII photoionization edges are 0.35 and 0.25 in NGC 1068, respectively. The same limits are 2.7 and 1.5 in the low Galactic latitude (and therefore highly absorbed) Circinus Galaxy. Assuming that the scattering plasma is in the typical conditions of the “warm absorbers” observed in Seyfert 1 galaxies (Reynolds 1997; George et al. 1998), these values correspond to hydrogen column densities of $N_{\text{H,warm}} \lesssim 5 \times 10^{21} \text{ cm}^{-2}$ and $N_{\text{H,warm}} \lesssim 4 \times 10^{22} \text{ cm}^{-2}$, broadly in agreement with the above diagnostics.

5.3 On the nature of the soft X-ray continua

In both Circinus Galaxy and NGC 1068, the soft X-rays continuum is most convincingly explained as the superposition of two components (even if for Circinus the evidence for a second component is marginal): a scattered power-law, which mirrors a fraction f_s of the primary nuclear emission; and an optically thin plasma emission, which we tentatively associate with a nuclear starburst. Indeed, both galaxies exhibits strong star-forming activity both in optical and IR (Scofield 1988; Maiolino et al. 1998).

Typical temperatures are $\simeq 0.4\text{--}0.5$ keV. They are slightly lower than those (0.6–0.9 keV) observed in starburst galaxies by ASCA (Ptak et al. 1999) and BeppoSAX (Persic et al. 1998; Cappi 1999). David et al. (1992) studied the correlation between far-infrared (FIR) and X-ray luminosity in starburst galaxies and derived a logarithmic scale law. The FIR luminosity of NGC 1068 (calculated assuming the formula (1) in David et al. 1992) is 2.2×10^{44} (Soifer et al. 1989); it translates into an expected 0.5–4.5 keV luminosity of $\sim 10^{41} \text{ erg s}^{-1}$, which is roughly consistent with that of the thermal component *alone* ($3.7 \times 10^{41} \text{ erg s}^{-1}$, given also the admittedly wide spread in the correlation. For Circinus Galaxy the integrated IR luminosity measured ($4 \times 10^{43} \text{ erg s}^{-1}$, Moorwood et al. 1996; Maiolino et al. 1998) corresponds to an expected X-ray luminosity of $\sim 2.1 \times 10^{40} \text{ erg s}^{-1}$, again broadly consistent with the observations. This evidence strengthens the case for the identification of this soft thermal component with the starburst. However, in Circinus Galaxy we cannot rule out the possibility that the excess emission is partly or entirely due to contaminating X-ray sources in the bulge of the galaxy.

In NGC 1068 the thermal component abundance is more than one order of magnitude lower than solar and in agreement with the value derived from the ASCA data (Netzer & Turner 1997). Similar values have been measured in starburst galaxies observed by ASCA (Ptak et al. 1998) and attributed to the relative weakness of the iron L complex lines. When the X-ray spectra of these galaxies are fitted with thermal plasmas, and the abundances of iron and α -elements are decoupled, the α -elements abundance recovers solar or even over-solar values (Persic et al. 1998), whereas the iron abundance remains robustly sub-solar (Cappi et al. 1999). This low metallicity is possibly due to iron depletion in warm interstellar clouds surrounded by a dust-rich galactic environment (Ptak et al. 1997). In principle, dilution by featureless continua, which may be provided by an unresolved population of accretion-driven sources, may explain

ems effect as well. These sources can be binaries in the nuclear starburst environment or in the host galaxy, spatially confused with the soft X-ray emission. There is clear evidence that the nuclear stellar population in NGC 1068 is relatively young ($\sim 5\text{--}35$ Myr; Davies et al 1998) and, therefore, a large contribution by High Mass X-ray Binaries (HMXRB) is expected. HMXRB are, however, generally flatter in the intermediate X-rays than NGC 1068 and, if they contribute significantly to the soft X-ray flux, their summed emission should dominate above 1 keV; this is not observed in the data. Alternatively, wind accreting Low Mass X-ray Binaries (LMXRB) are harder and soft X-ray brighter. In “normal” spiral galaxies like our own and M 31 (Trinchieri & Fabbiano 1991), they indeed dominate the total X-ray output, with an integrated X-ray luminosity in the range $10^{39}\text{--}10^{41}$ erg s $^{-1}$; the brightest sources generally cluster around the galactic bulge. Of course, the soft X-ray spectrum might well be more complex than our simple, statistical-limited two-components deconvolution. BeppoSAX and ASCA results, although obtained with detectors having relatively modest energy resolution, are suggestive of a very complex situation, which will be clarified by the forthcoming major X-ray missions like *Chandra*, XMM and Astro-E, whose high resolution soft X-ray detectors will surely shed a new light on this subject.

ACKNOWLEDGMENTS

This paper has made use of linearized event files produced at the BeppoSAX Science Data Center. The following institutions are acknowledged for financial support: European Space Agency (MG, research fellowship), Italian Space Agency (GM, RM, AM, FF), MURST (GM), Royal Society (ACF), PPARC (KI). We thank the referee the valuable comments which helped us in clarifying several issues.

REFERENCES

- Anders E., Grevesse N., 1989, *Geochimica and Cosmochimica Acta*, 53, 197
 Antonucci R., Miller J.S., 1985, *ApJ*, 297, 621
 Antonucci R., 1993, *ARAA*, 31, 473
 Awaki H., Koyama K., Inoue H., Halpern J.P., 1991, *PASJ*, 43, 195
 Boella G., Butler R., Perola G.C., 1997a, *A&AS*, 112, 299
 Boella G., et al., 1997b, *A&AS*, 223, 327
 Cappi M., Bassani L., Comastri A., et al., 1998, *A&A*, in press
 Cappi M., 1999, *Adv. Sp. Res.*, submitted
 Cappi M., et al., 1999, *MmSAIt*, in press (*astroph/9809325*)
 Claussen M.J., Heiligman G.M., Lo K.Y., 1984, *Nature*, 310, 298
 Cusumano G., Mineo T., Guainazzi M., et al., 1998, *A&A*, submitted
 David L.P., Jones C., Forman W., 1992, *ApJ*, 388, 82
 David L.P., Harnden F.R. Jr., Kearns K.E., Zombeck M.V., 1996, “The ROSAT High Resolution Imager (HRI) Calibration Report”, U.S.ROSAT SDC/SAO
 Davies R.I., Sugai H., Ward M.J., 1998, *MNRAS*, 300, 388
 Dickey J.M., Lockman F.J., 1990, *ARA&A*, 28, 215
 Fiore F., Guainazzi M., Grandi P., 1998, “The cookbook for BeppoSAX NFI Spectral Analysis”, in press
 Frontera F., Costa E., Dal Fiume F., Feroci M., Nicastro L., Orlandini M., Palazzi E., Zavattini G., *A&AS*, 112, 357
 George I.M., Fabian A.C., 1991, *MNRAS*, 249, 352

- Yaqoob T., 1998, *ApJS*, 114, 73
 Ghisellini G., Haardt F., Matt G., 1994, *MNRAS*, 267, 743
 Giommi P., Angelini L., Jacobs P., Tagliaferri G., in “Astronomical Data Analysis Software System I”; Worral D.M., Biemesderfer J., Barnes J. eds, 1991, *A.S.P.Conf.Ser.*, 25, 100
 Grandi P., et al., 1997, *A&A*, 325, L17
 Greenhill L.J., Gwinn C.R., Antonucci R., Barvanis R., 1996, *ApJ*, 472, L21
 Greenhill L.J., Ellingsen S.P., Norris R.P., Gough R.G., Sinclair M.W., Moran J.M., Mushotzky R.F., 1997, *ApJ*, 474, L103
 Haardt F., et al., 1998, *A&A*, 340, 35
 Heisler C.A., Lumsen S.L., Bailey J.A., 1997, *Nature*, 385, 700
 Kikoin I.K. (ed), 1976, *Tables of Physical Quantities*, Atomizdat, Moscow
 Krolik J.H., Kallman T.R., 1987, *ApJ*, 320, 5
 Krolik J.H., Madau P., Życki P.T., 1994, *ApJ*, 420, 57
 Iwasawa K., Fabian A.C., Matt G., 1997, *MNRAS*, 289, 443
 Iwasawa K., Comastri A., 1998, *MNRAS*, 297, 1219
 Magdziarz P., Zdziarski A.A., 1995, *MNRAS*, 273, 837
 Maiolino R., Ruiz M., Rieke G.H., Keller L.D., 1995, *ApJ*, 446, 561
 Maiolino R., Krabbe A., Thatte N., Genzel R., 1998a, *ApJ*, 493, 650
 Maiolino R., Salvati M., Bassani L., Dadina M., Della Ceca R., Matt G., Risaliti G., Zamorani G., 1998, *A&A*, 338, 781
 Malaguti G., Palumbo G.C.C., Cappi M., Comastri A., Otani C., Matsuoka M., Guainazzi M., Bassani L., Frontera F., 1998, *A&A*, 331, 519
 Manzo G., et al., 1997, *A&AS*, 112, 341
 Marconi A., Moorwood A.F.M., Salvati M., Oliva E., 1994, *A&A*, 291, 18
 Marshall F.E., et al., 1993, *ApJ*, 405, 168
 Matt G., Piro L., Antonelli L.A., Fink H.H., Meurs E.J.A., Perola G.C., 1994, *A&A*, 292, L13
 Matt G., Brandt W.N., Fabian A.C., 1996a, *MNRAS*, 280, 823 (*MBF96*)
 Matt G., Fiore F., Perola G.C., Piro L., Fink H.H., Grandi P., Matsuoka M., Oliva E., Salvati M., 1996b, *MNRAS*, 281, 69
 Matt G., et al., 1997a, *A&A*, 325, L13 (*M97*)
 Matt G., Fabian A.C., Reynolds C.S., 1997b, *MNRAS*, 289, 175
 Matt G., Guainazzi M., Maiolino R., et al., 1999, *A&A*, 341, L39 (*M99*, *astroph/9811301*)
 Miller J.S., Goodrich R.W., Mathews W.G., 1991, *ApJ*, 378, 47
 Moorwood A.F.M., Lutz D., Oliva E., Marconi A., Netzer H., Genzel R., Sturm E., De Graauw T., 1996, *A&A*, 315, L109
 Mulchaey J.S., Koratkar A., Ward M.J., Wilson A.S., Whittle M., Antonucci R.R.J., Kinney A.L., Hurt T., 1994, *ApJ*, 436, 586
 Nandra K., George I.M., Mushotzky R.F., Turner T.J., Yaqoob Y., 1997, *ApJ*, 477, 602
 Nandra K., Pounds K.A., 1994, *MNRAS*, 268, 405
 Netzer H., Turner T.J., 1997, *ApJ*, 488, 694
 Netzer H., Turner T.J., George I.M., 1998, *ApJ*, 504, 680 (*NTG98*)
 Nicastro F., Elvis M., Fiore F., Perola G.C., 1998, *ApJ*, in press (*astroph/9808316*)
 Oliva E., Marconi A., Cimatti A., di Serego Alighieri S., 1998, *A&A* 329, L21
 Orr A., Parmar A.N., Yaqoob T., Guainazzi M., 1998, *Nucl. Phys. B (Proc. Suppl.)*, 69/1-3, 496
 Parmar A.N., et al., 1997, *A&AS*, 122, 309
 Persic M., et al., 1998, *A&A*, 339, 33
 Piro L., et al., 1998, *Nucl. Phys. B (Proc. Suppl.)*, 69/1-3, 481
 Ptak A., Serlemitsos P., Yaqoob T., Mushotzky R., Tsuru T., 1997, *AJ*, 113, 1286
 Ptak A., Serlemitsos P. Yaqoob T., Mushotzky R., 1999, *ApJS*, in press (*astroph/9808159*)
 Reynolds C.S., 1997, *MNRAS*, 286, 513

Scoville N.Z., 1988, *ApJ*, 327, 61
 Soifer B.T., Bohemer L., Neugebauer G., Sanders D.B., 1989, *AJ*, 98, 766
 Smith D.A., Done C., 1996, *MNRAS*, 180, 355
 Tran H.D., 1995, *ApJ*, 440, 565
 Trinchieri G. & Fabbiano G., 1991, *ApJ*, 382, 82
 Tully R.B., 1988, “Nearby Galaxies catalog”, Cambridge University Press
 Turner T.J., George I.M., Nandra K., Mushotzky R.F., 1997a, *ApJ*, 488, 164
 Turner T.J., George I.M., Nandra K., Mushotzky R.F., 1997b, *ApJS*, 113, 23
 Ueno S., Mushotzky R.F., Koyama K., Iwasawa K., Awaki H., Hayashi I., 1994, *PASJ*, 46, L71
 Ueno S., 1997, Ph.D. thesis, Kyoto University
 Wilson A.S., Elvis M., Lawrence A., Bland-Hawthorn J., 1992, *ApJ*, 391, L75
 Zdziarski A.A., Johnson W.N., Done C., Smith D., McNaron-Brown K., 1995, *ApJL*, 438, 63